Dynamic global model of Cl2/Ar plasmas: Applicability to atomic layer etching processes

T. Rasoanarivo, C. Mannequin, F. Roqueta, M. Boufnichel, A. Rhallabi

Dynamic global model of Cl_2/Ar plasmas: applicability to Atomic Layer Etching processes

T.Rasoanarivo,[1,2] C.Mannequin,[1] F.Roqueta,[2] M.Boufnichel,[2] and A. Rhallabi[1]

[1)] *Nantes University, CNRS, - Institute of Materials of Nantes Jean Rouxel, IMN, F-44000 Nantes, France*

[2)] *STMicroelectronics Tours - 10 Rue Thalès de Milet, 37100 Tours, France.*

(*Electronic mail: tojo.rasoanarivo@cnrs-imn.fr)

(Dated: 25 September 2024)

A global zero-dimensional (0D) model has been developed to describe the Cl_2/Ar plasma discharge in dynamic mode. Our model computes the time evolution of the plasma composition under conditions similar to fast-paced plasma processes, such as Atomic Layer Etching (ALE), characterized by alternations in the feed gas. The study focuses on calculating the densities of charged and neutral species for various gas switch durations, (t_s). Simulations demonstrate the impact of gas switching time (t_s) on the temporal evolution of Cl_2, Cl, and ion densities, as well as the electron temperature (T_e) during the gas switch. A parametric study reveals that the temporal evolution of T_e can be represented by a semi-empirical exponential law during the transition from a pure Cl_2 plasma to Ar as a function of (t_s). During the gas switch, the extinction of chlorinated species, which play a crucial role in the adsorption step in ALE, persist during the argon plasma phase. The duration of this extinction decreases with longer ts. Finally, our model shows a good reproducibility of ALE cycles modeled for the chosen input parameters, including the densities of neutral and charged species and T_e, relative to the ALE period. This work aims to provide insights into the kinetics of transient plasmas occuring in ALE cycle ALE cycle, the importance of purging, and lifetime residual species, such as residual chlorine in a plasma with pure argon.

I. INTRODUCTION

Plasma etching processes are widely employed in the manufacturing of electronic and optoelectronic devices such as microprocessors, memory circuits, and amplifiers.[1] Advancements in scaling down these devices demand a higher level of precision in pattern transfer while minimizing structural defects, especially within the devices' active zones. For instance, the electrical performance of GaN-based High Electron Mobility Transistors (HEMTs) heavily relies on

minimizing the morphological and stoichiometric defect density introduced during the etching steps for gate formation between the drain and the source.[2]. Plasma Atomic Layer Etching (ALE) emerges as a promising alternative, capable of meeting such stringent specifications.[3]. Plasma ALE is a cyclic etching process designed to precisely etch only one monolayer of a target material per cycle. An ideal plasma ALE cycle comprises two self-limiting half-reactions enabled by alternating gas pulses, often separated by purge steps. The first half-reaction involves the surface modification of the uppermost atomic layer of the material, through the adsorption of neutrals and radicals from a reactive gas-based plasma. The second half-reaction involves the controlled and selective removal of the previously modified layer without damaging the underlying unmodified layers. This second reaction is often achieved by controlled energetic ion bombardment from a rare gas plasma.[4–7] Most reported ALE processes also utilize the rare gas from the second half-reaction as a purge gas while maintaining the plasma discharge during the purge steps that separate the two half-reactions.[8] Such process entails the continuous exposure of the material surface to plasmas. Since ALE is ideally control at the atomic-scale, plasma deviation has the potential to impact the process, particularly when ALE steps are conducted in disparate plasma media. While a global model has been developed in steady-state for a constant plasma mixture, the species densities can be tracked for gas pulsed plasmas in a dynamic mode. Plasma of varying composition during the transitions occurring from the modification to the first purge step, that we will refer to transient plasmas, could alter the controlled modification reactions by over-exposing the surface to unquantified or undesired fluxed of modifying species. In particular, the densities and residence time of the species (neutrals, ions and radicals) in these transient plasmas have to be investigated. On the other hand, these varying fluxes of modifying species could be integrated into the overall surface modification scheme as recently proposed by Fathzadeh et al for the concept of Transient-assisted plasma etching.[9] This work aims to model low-pressure plasma discharges composition during these transitions occurring in ALE process and could highlight the possible sources of deviation processes.

ALE of various materials of choice for the microelectronics industry has been achieved with chlorine based chemistries: Cl_2 or BCl_3 as a source of reactive species for the modification step while a rare gas based plasma like argon is used for the ion bombardment step.[3,10,11]

Several studies have been carried out to model low-pressure plasma discharges based on chlorine. Notably, 2D models employing a fluid approach for modelling Cl_2 plasmas or Cl_2-based mixtures ,[12–15] providing information about the spatial variation of electron density, ion and neutral densities at the plasma phase, as well as the electron temperature. These approaches while providing a detailed plasma description are still time-consuming. Other works also focus on plasma kinetic models of Cl_2-based mixtures using a global approach have been developed.[16–23] All of those studies are

mainly carried out for modelling Reactive Ion Etching (RIE) processes of silicon or III-V materials such as InP.[18] The main advantage of a global kinetic model is its ability to use a quite extensive reaction scheme occurring simultaneously at the plasma discharge. The computational run using such approach is much faster compared to those using the fluid model[12,13] or a Particle In Cell (PIC) one.[24–26] In Inductively Coupled Plasma (ICP), most of the global kinetic models have been developed in the radio-frequency domain with a continuous feed gas injection.

To date, global models have been well used to determine the plasma composition at plasma reactor parameters, which have been first designed to describe plasma in steady-states conditions.[17,23]

In this present study, we propose a dynamic global model of Cl_2/Ar plasmas that follows the evolution of the plasma over time during a complete ALE cycle, adsorption, purge, activation and purge while modelling the feed gas switch overtime. The global kinetic model is applied for an alternating feed gas Cl_2/Ar to simulate the ALE conditions (Cl_2 plasma discharge to Ar)

II. COMPUTATIONNAL MODEL

As described in the previous section, the 0D global approach is used to model Cl_2/Ar plasma kinetics. Details of our global kinetic model are presented in previous works[17–19,27] where simulations are performed only in stationary conditions for Cl_2/Ar plasma mixture.

The model used in this work has been upgraded from the last version published in the work of Le Dain et al.[27] Whitout any modifications in the reaction scheme. Consequently, the pressure is calculated at each time step, and self-consistent to the value of the first input. Firstly, the model is used to calculate plasma parameters and densities for various Cl_2/Ar compositions in steady-state conditions. It is then employed to calculate plasma properties of transient Cl_2/Ar plasma where the feed gas composition varies over time in dynamic mode of the global model. It allows investigating the kinetic of the transient plasma occurring during the transition from an ALE modification step (i.e. a pure Cl_2 plasma) to the purge step (i.e. a pure Ar plasma). Afterward, it is applied in ALE conditions by studying the temporal transition from a pure Cl_2 to a pure Ar plasmas, modelled as a temporal feed gas switch. The kinetic model relies on the continuity equations for each neutral and ion species under consideration:[17,18]

$$\begin{aligned}\frac{\partial n_i}{\partial t} =& \delta_i \left(x_i(t) \frac{Q}{V} \right) - \sum_l k_{el}(T_e) n_i n_e + \sum_n k_{en}(T_e) n_m n_e \\ & - \sum_m k_{mi}(T_g) n_i n_m + \sum_{lm} k_{ml}(T_g) n_l n_m - k s_i n_i \\ & + k s_l n_l - \frac{n_i}{\tau_P}\end{aligned} \tag{1}$$

where, the first term corresponds to the inlet feed gas. In our case, $\delta_i = 1$ for $i = Cl_2, Ar$ and $\delta_i = 0$ for the other species. $x_i(t)$ is time evolution of the flow rates fraction of both Cl_2 and Ar, V is the reactor chamber volume and Q is the total flow rate. Fig. 1 presents one example of the $x_{Cl_2}(t)$ and $x_{Ar}(t)$ time evolution which allows the simulation of the transition from a pure Cl_2 plasma to a pure Ar plasma. The 2^{nd} and 3^{rd} terms correspond to the loss and the production rate of the species i by electronic impact where k_{el} are the reaction coefficients of reactions l by electronic impact.

To calculate the reaction coefficients by electronic impact, the Boltzmann equation has to be solved. Electron impact reaction coefficients by electronic impact depend on the effective cross-sections extracted from the literature. The reaction coefficients are calculated using the following formula:

$$k(T_e) = \langle \sigma(\epsilon) v_e \rangle = \int_0^{\inf} \sqrt{\frac{2\epsilon}{m_e}} \sigma(\epsilon) f(\epsilon, T_e) d\epsilon \tag{2}$$

where $\mathrm{T_e}$ is the electron temperature, $\mathrm{v_e}$ is the electron velocity, $\mathrm{m_e}$ is the electron mass, $f(\epsilon)$ is the electron energy distribution function (EEDF), and ϵ is the electron kinetic energy. In this study, the electron impact reaction coefficients are determined by approximating the EEDF with a Maxwellian distribution. The latter is expressed as a function of energy and electron temperature $\mathrm{T_e}$:

$$f(\epsilon, T_e) = \sqrt{\frac{8}{\pi m_e}} \epsilon (q T_e)^{-\frac{3}{2}} \exp\left(-\frac{\epsilon}{q T_e} \right) \tag{3}$$

By integration Eq. 2, $\mathrm{k(T_e)}$ associated to all electronic impact reactions are obtained.

The 4^{th} and ^{5th} terms represent the loss and production rates by reactions of the considered species $i - m$ and $m - l$ respectively, where k_{mi}/k_{ml} is the associated kinetic coefficient calculated as a function of the gas temperature, $\mathrm{T_g}$. The 6^{th} term corresponds to the loss rate of species i on the reactor walls and the 7^{th} is the production term of the reaction wall where ks_l is the surface reaction coefficient of species l. Such coefficients are calculated, for the neutral

species, as a function of the diffusion coefficient using Chantry theory.[28] The last term corresponds to the loss term of species i by pumping. The real time plasma pressure p, according to the ideal gas law as the sum of partial pressures, is given by:

$$p = k_B T_g \sum_i n_i \tag{4}$$

where n_i corresponds to all of the distinct species densities in the gas, k_B is the Boltzmann constant and T_g is the gas temperature. As the heating equation is not included in our model for the estimation of the gas temperature, we use a semi-empiric relation where the gas temperature is a function of the plasma pressure and the RF power, detailed in previous work from Thorsteinsson et al.[29]

The charge neutrality equation is added to self-consistently determine the electron density:

$$n_e + \sum_j n_{-,j} = \sum_i n_{+,i} \tag{5}$$

where $n_{-,j}$ and $n_{+,i}$ are the densities of negatives j and positives i ions respectively.

Finally, a power continuity equation is considered to determine the electron temperature T_e by the following equation:

$$\frac{\partial(\frac{3}{2} q T_e n_e)}{\partial t} = \frac{\eta P_{RF}}{V} - (P_{ev} + P_{ew} + P_{Ions,w}) \tag{6}$$

Where, q is the electron charge, P_{RF} is the RF source power applied to the antenna and $\eta = 0.9$ is the estimated effective power fraction absorbed by the electrons. P_{ev}, P_{ew} and $P_{Ions,w}$ are the power losses between the electron-neutral, electron wall and ion wall collisions respectively. P_{ev} is determined by considering electron-species collision. The term $P_{e,Ions,w} = P_{ew} + P_{Ions,w}$ is calculated by considering the average energy per electron or ion respectively during a collision with the reactor walls.

$$P_{ev} = n_e \left(\sum_{i,j} \epsilon_{j,(+,i)} k_{j,(+,i)} n_j + \sum_{j,l} \epsilon_{jl} k_{jl} n_j + \sum_{j} \frac{3kT_e m_e}{M_j} k_{j,el} n_j \right) \tag{7}$$

$$P_{e,Ions,w} = \sum_{j} k s_j n_{+,j} (\epsilon_{Ions,w,j} + \epsilon_{ew}) \tag{8}$$

In Eq. 7, $\epsilon_{j,(+,i)}$ and ϵ_{jl} are the threshold energies for ionization and excitation of species j to species i or l respectively. M_j is the mass of the neutral species j and m_e is the mass of an electron. For equation 8, $\epsilon_{Ions,w,j}$ and ϵ_{ew} are respectively the average energies lost by ions and electrons at the reactor walls. In this global model, $\epsilon_{Ions,w,j}$ and ϵ_{ew} are approximated by $2qT_e$ and $6qT_e$ respectively. Ions energy is set constant at 0.5 eV.[16]

As previously mentioned, we implemented a dynamic mode in our 0D plasma model especially during the transition from a pure Cl_2 plasma to a pure Ar one. As a first approximation, we consider a linear time ramp corresponding to a change in the feed gas composition of the Cl_2/Ar while maintaining a constant total flow rate. The linear temporal progression from pure Cl_2 to pure Ar plasma starts at t_{sb} and ends at t_{se}, leading to a switch duration of t_s=t_{se}-t_{sb}.Experimentally, t_s can vary from few milliseconds to the second. It is relevant to study the plasma kinetic for t_s= [0.001:4] s. Others functions such as step-by-step or exponential could also be good approaches in regards of a mass flow meter's time response.

The steady-state condition is reached when the plasma properties represented by ni, ne and Te reach constant values with time, i.e. $\frac{\partial n_i}{\partial t} = \frac{\partial n_e}{\partial t} = \frac{\partial T_e}{\partial t} = 0$. In dynamic mode, employed to investigate transient plasma arising from feed gas switching from pure Cl_2 to pure Ar, the plasma properties are reported as time dependent functions as the balance equations are non-null, i.e. $\frac{\partial n_i}{\partial t} = \frac{\partial n_e}{\partial t} = \frac{\partial T_e}{\partial t} \neq 0$.

According to Eq. 4, the residence time is calculated considering the instantaneous pressure fluctuation due to the time variation of the total particle density:

$$\tau_P(t) = \frac{V}{Q} \times \frac{k_B T_g \sum_i n_i(t)}{P_{atm}} \tag{9}$$

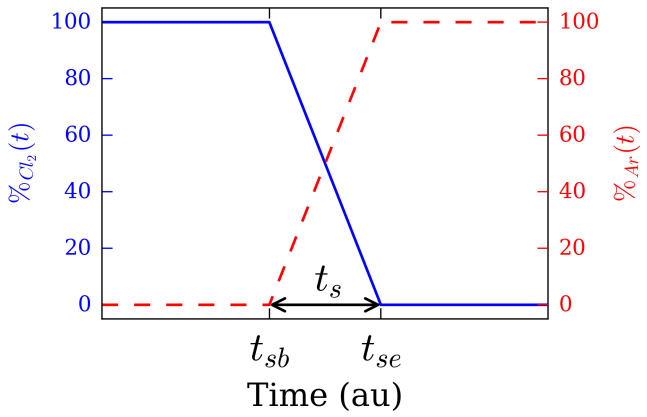

FIG. 1: Representation of the time evolution of $\%Cl_2$ and %Ar, percentage of Cl_2 and Ar of the total flow rate respectively during the feed gas switch from t_{sb} to t_{se}. This occurs during the transition between modification step (Cl_2 plasma) and purge/activation step (Ar plasma). Total flow rate remains constant.

where $n_i(t)$ is the instantaneous neutral or ion density, T_g is the gas temperature and k_B is the Boltzmann constant. The variation of τ_P with time induces a long calculation time compared to the previous model version where the residence time was determined from the initial pressure input of the calculation. The global model is coded in Fortran77, and the nonlinear differential equation system is solved using a LSODE, the Livermore solver for ordinary differential equations.[30]

III. RESULTS AND DISCUSSIONS

A. steady-state conditions

Plasmas modeling has been widely studied since thirty years.[16] Firstly, simulations have been performed for various Cl_2/Ar plasma mixture in steady-state condition composition in order to validate our reaction scheme and improved model. Results are compared with the modeling and experimental works of Efremov et al.[23] and Thorsteinsson et al.[29]

Figure 2 presents the charged and neutral densities as well as the electron temperature as a function of $\%Cl_2$ in Cl_2/Ar plasmas in steady-states conditions for $P_{RF} = 800$ W , total flow rate Q = 60 sccm, pressure p = 1.33 Pa and wall temperature $T_w = 300$ K.

The electron density increases from 7.6×10^{10} cm^{-3} to 3.1×10^{11} cm^{-3} when decreasing $\%Cl_2$. Cl_2 is an electronegative gas for which dissociative attachments upon electronic collisions can occur at relatively low energy,[31] leading to a steady increase of the Cl^- density, which becomes the main negative species for $\%Cl_2$ above 60%.

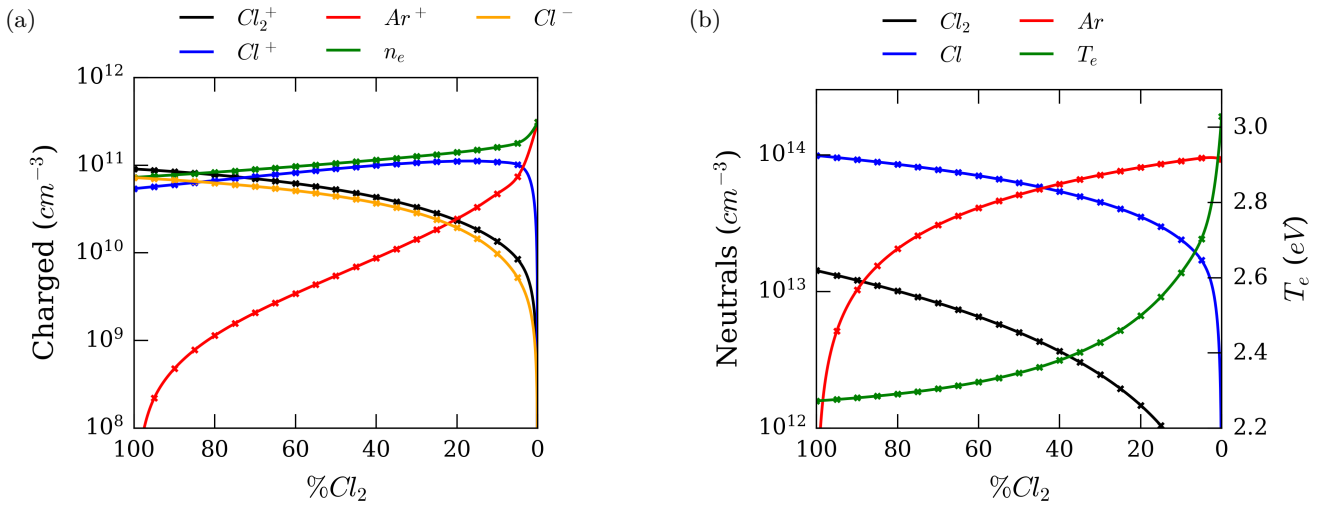

FIG. 2: Species densities for steady-state simulations of Cl_2/Ar plasma at p = 1.33 Pa, P_{RF} = 800 W, Q = 60 sccm and T_w = 300 K,(a) charged species and (b) neutrals and T_e.

The electron temperature T_e increases from 2.34 eV to 3.02 eV as the $\%Cl_2$ decreases. For chlorine rich plasma, i.e., above $60\%Cl_2$, a significant part of electrons energy is dissipated through electronic collisions: dissociation and/or excitation processes, such as rotational and vibrational excitations of Cl_2, leading to an overall decrease of electrons kinetic energy i.e., T_e. Owing to the high T_e and n_e, the dissociation of Cl_2 into Cl radicals is enhanced in argon rich plasma as reported in Fig. 3. The Cl^+ density increases with the diminution of $\%Cl_2$ until reaching a maximum around $20\%Cl_2$. This is due to the increase of ne and Te for lower $\%Cl_2$, leading to an increased ionization rate of Cl and dissociation rate of Cl_2, even though Cl and Cl_2 densities continue to decrease with the diminution of $\%Cl_2$. In the [60-10] $\%Cl_2$ interval, Cl^+ is the dominant positive ion, while for $\%Cl_2 < 10\%$, Ar^+ is the dominant ion and for $\%Cl_2 > 80\%$, Cl_2^+ is dominant. Conversely, Cl^- density increases with $\%Cl_2$ and exceeds Ar^+density for $\%Cl_2 > 40\%$.

We report in Fig 3-a, the main kinetic coefficients for the Cl_2 dissociation reaction by electronic collisions versus T_e. At T_e lower than $1eV$, the dissociative attachment is favored, but significantly decreases at higher T_e. For T_e above $1eV$, the others dissociation reactions are amplified as T_e rises. Such trends are the main phenomena responsible for the high Cl density observed for Ar rich plasma (see Fig. 2). On the other hand, the decrease of T_e for Cl_2 rich plasma lowers Cl_2 dissociation efficiency.

Figure 4 reports normalized densities from Efremov et al.[23], reported as cross markers for densities measured by

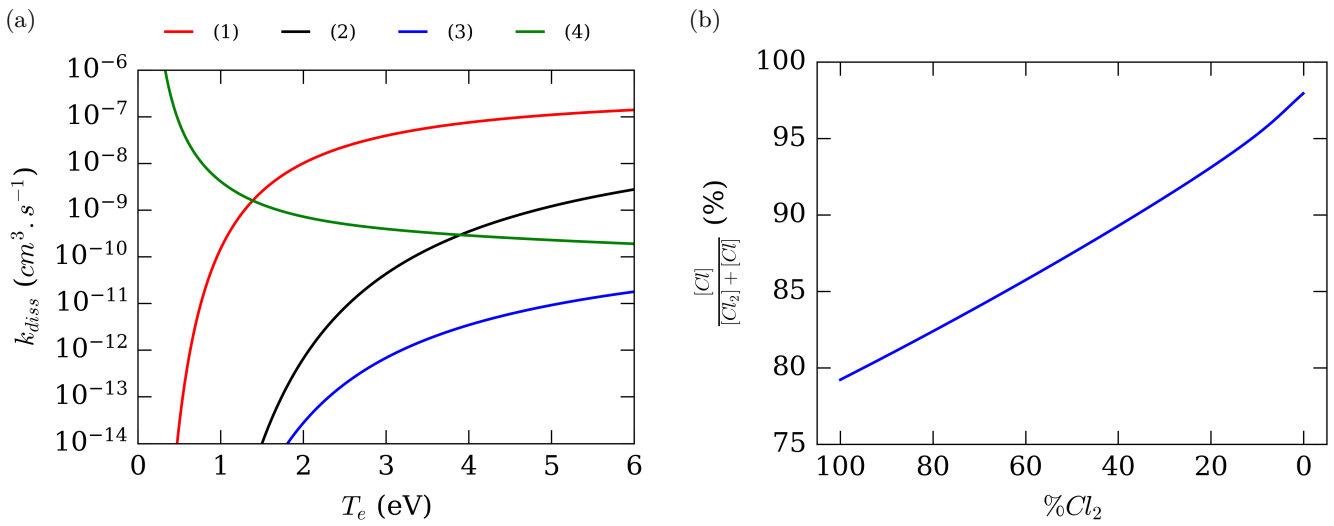

FIG. 3: (a) Kinetic coefficients of Cl_2 dissociation reactions by electronic impact versus T_e at p = 1.33 Pa, P_{RF} = 800 W, Q = 60 sccm and T_w = 300 K. (1) $Cl_2 + e \rightarrow 2Cl + e$, (2) $Cl_2 + e \rightarrow Cl^+ + Cl + 2e$, (3) $Cl_2 + e \rightarrow Cl^+ + Cl^- + e$,(4) $Cl_2 + e \rightarrow Cl + Cl^-$, (b) dissociation rate of Cl_2 against the feed gas composition for the same parameters.

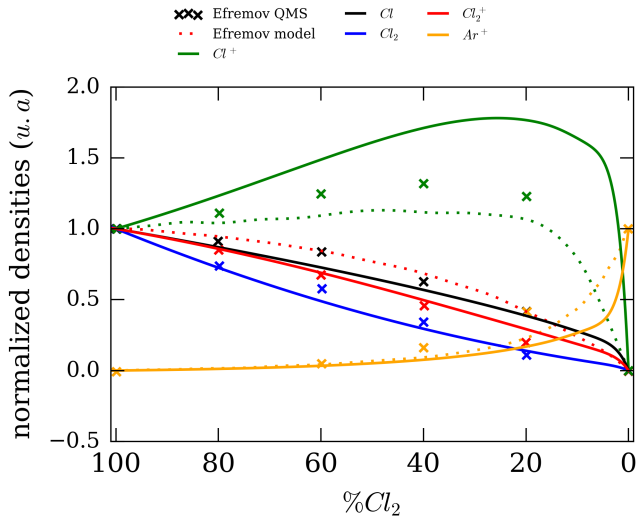

FIG. 4: Comparison of QMS measurements and simulation results of densities from Efremov et al.[23] in Cl_2/Ar plasma with our model set at identical input parameters (P_{RF} = 700 W and p = 0.53 Pa). Solid lines: our computational results, dashed lines: computational results from Efremov et al.[23] and markers: QMS results

Quadrupole Mass Spectroscopy (QMS) and as dashed lines for simulated ones. Results of our computational work are also presented for identical inputs conditions, reported as solid lines. Each density has been normalized to their own maximum. Chlorine densities have been normalized by their values calculated or measured at 100%Cl_2, similarly argon ion density has been normalized by its value calculated or measured at 0%Cl_2.

The normalized Cl^+ density obtained from our model progressively increases as $\%Cl_2$ decreases up to reaching a maximum at $25\%Cl_2$, and then gradually decreases up to $5\%Cl_2$ and finally collapses as the composition tends towards $0\%Cl_2$. The normalized Cl^+ density from our calculation departs from the normalized calculated Cl_+ density from Efremov model, but follows a similar trend as their experimental results. The difference between the two normalized calculated densities may originate from a higher dissociation of the Cl_2 in low $\%Cl_2$ supported by higher n_e and T_e in our calculation. In addition, our model considers Cl recombination into Cl_2 in volume and additional volume reactions Cl comparing with Efremov reaction scheme (see R52-R53 in reaction scheme). The latter may lead to a higher Cl_2 dissociation degree especially at low $\%Cl_2$ favoring the ionization of Cl into Cl^+. Moreover, our model has been improved regarding the management of physical parameters, such as pressure, with a self-consistent function of the pumping term (see Eqs. 4 and 9 and the gas temperature function from Thorsteinsson et al. work.[29]

Our results present the same qualitative hierarchy for the reported normalized chlorine densities: $Cl > Cl_2^+ > Cl_2$. The normalized Ar^+ density from our simulation follows the same downward trend as the density simulated by Efremov and the corresponding QMS measurements. Our simulation results reveal a sharper decrease of the normalized Ar^+ density with $\%Cl_2$ regarding Efremov's results. Compared with Efremov, it originates from a faster decline of the n_e and T_e as discussed above.For further validation, our model is also confronted to Thorsteinsson et al.28 work, for the same machine parameters, presented in Figs. 5 and 6.

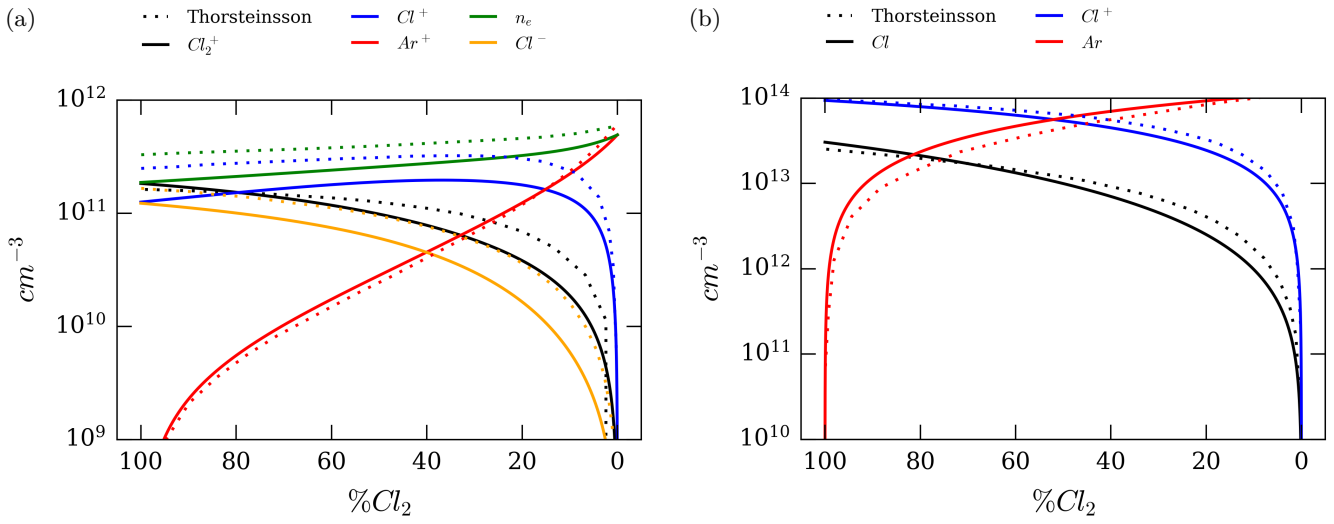

FIG. 5: (a) Charged and (b) neutral species densities versus $\%Cl_2$ for p = 1.33 Pa, P_{RF} = 500 W, Q = 100 sccm, R = 10 cm, L = 10 cm. Solid lines: our model, dashed lines: as Thorsteinsson model.[29]

Figure 5 shows the simulation results from our model compared to those of Thorsteinsson et al.28 Contrary to Fig.

4, which presents normalized data, absolute densities of neutral and charged species are presented versus $\%Cl_2$. These results, in solid lines, align well with those presented in Figure 2 at different machine parameters. A good agreement between our model and those from Thorsteinsson et al.[29] is observed. The trends for species densities are consistent, but the amplitude of each chlorine species is slightly lower in our model, favoring argon species. Additionally, our model shows a lower dissociation rate of Cl_2 in highly chlorinated plasma, resulting in overall lower atomic chlorine species

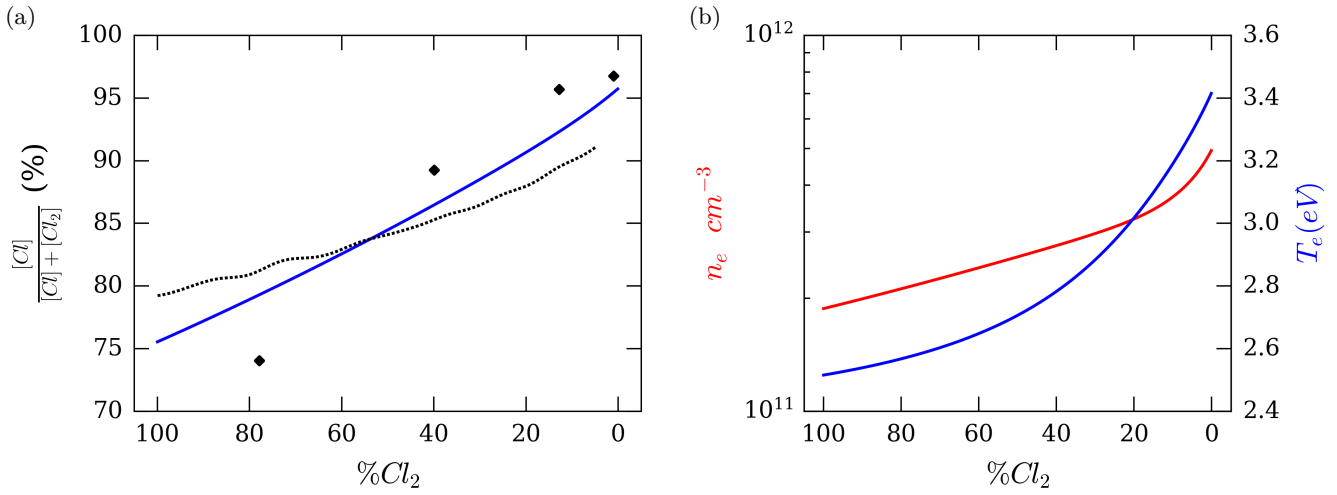

FIG. 6: (a) Dissociation rate of Cl_2 of our results (solid line) compared to Thorsteinsson et al.[29] model dissociation (dotted line) and Fuller et al.[32] dissociation rate (black diamonds) obtained by optical actinometry for p = 2.4 Pa, Q = 38 sccm, P_{RF} = 600 W. (b) Electron density and temperature versus $\%Cl_2$ for the same parameters in our model.

Figure 6-a presents the dissociation rate evolution of the Cl_2 versus $\%Cl_2$ determined by our model and compared with Thorsteinsson et al.[29] work. Both of the models show similar trends for the calculated densities. The increase of the dissociation rate of Cl_2 is due to the increase of n_e and T_e when decreasing $\%Cl_2$ (Fig. 6-b). The simulation results reveal that our calculated dissociation rates of Cl_2 are close to those obtained experimentally by Fuller et al. using optical actinometry[32] at different parameters, p = 2.4 Pa, Q = 38 sccm, and P_{RF} = 600 W, reported as markers in Fig. 6-a. The dissociation rate in our simulation results increases from 76% to 96% as $\%Cl_2$ decreases and is higher than Thorsteinsson's results when below $\%Cl_2$. However, this trend reverses when the $\%Cl_2$ exceeds 50%. The dissociation rate from our results aligns with those reported from the experiment.[32].

We conducted steady-state simulations for our global model with the objective of validating our improved model. A comparison of our results with those of Efremov et al.[23] reveals discrepancies that may be attributed to differing methodologies, particularly the volume recombination of Cl, which results in a higher dissociation degree in low

chlorinated plasma, in addition to the update of the pressure management. In comparison with the findings of Thorsteinsson et al.[29], our results demonstrate a satisfactory degree of alignment, despite a slight discrepancy in the calculated chlorine densities, in favor of the argon species. Furthermore, the dissociation rate of Cl_2 observed in our results exhibits a comparable trend to that reported by Thorsteinsson et al.[29], aligning with the dissociation rate proposed by Fuller et al.[32]

B. Feed gas switch : dynamics from Cl_2 to Ar plasma

In Cl_2/Ar-based Atomic Layer Etching (ALE), chlorine plasma is utilized for the modification step, while argon plasma is employed for the activation step. The objective of our study is to examine the plasma kinetic behavior within the ALE framework, particularly during the feed gas transition phase. This transition, illustrated in Fig. 1 of our model, marks the shift from the modification step to the removal step. We implemented a linear time ramp to correspond with the change in the Cl_2/Ar feed gas composition, ensuring a constant total flow rate throughout the process.

Figure 7 presents the charged and neutral species densities versus time during the feed gas switch starting at t_{sb} = 0.5 s and for a switch duration of t_s = 1 s in Fig. 7-a,b and t_s = 0.05 s in Fig. 7-c,d.

In Fig. 7-a and 7-b, the densities obtained for the dynamic mode exactly follow the trend of the steady-states for a feed gas switch duration t_s = 1 s. However, in Fig. 7-c and 7-d, we observe a discrepancy between the dynamic mode results and the steady-states. For a feed gas switch duration of t_s = 0.05 s, the results obtained in dynamic mode of our model does not have sufficient time to adapt to the feed gas switch from Cl_2 to Ar in temporal input parameters. Significant chlorine residuals are observed after the switch at t=t_{se}, with concentrations of 10^{13} cm^{-3} and 10^{10} cm^{-3} for Cl and Cl^+ respectively. These findings are critical in the context of ALE, particularly when transitioning from the modification step to the activation step, chlorine species could interfere with the Ar^+ sputtering.

The Ar^+, n_e densities and T_e increase with time during t_s. However after t_{se}, these densities still vary while reaching their steady-state in 100% argon feed gas. The differences between the densities' variations for t_s = 0.05 s and t_s = 1 s could indicate that the plasma kinetic is bounded from time when t_s is short.

We compare in Fig. 8, Cl_2, Ar and n_e densities as well as T_e obtained in dynamic mode (from blue to red, t_s = [0.001,0.01,0.05,0.1,0.25,0.5,1,2,3,4]s), with those corresponding to the steady-states, as black diamond markers, for identical %Cl_2 compositions in the feed gas source switch from Cl_2 to Ar (from 100%Cl_2 to 0%Cl_2). We describe in Fig. 1, the implementation of a dynamic mode corresponding to a temporal linear ramp of %Cl_2 of the feed gas input.

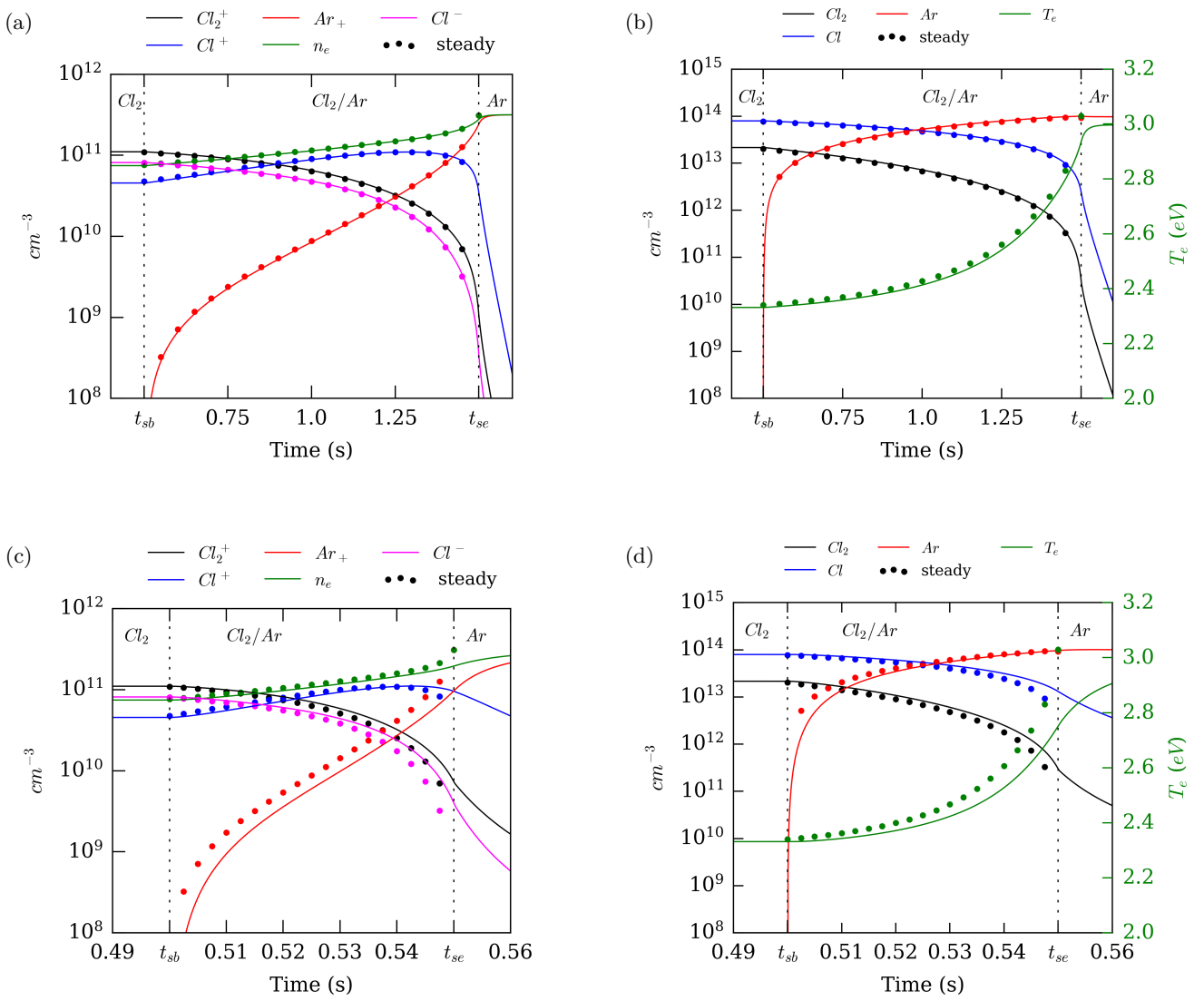

FIG. 7: Transient plasma densities during a feed gas switch from a pure Cl_2 plasma to a pure Ar Plasma for (a) Charged species and (b) neutral species and electronic temperature with $t_s = 1$ s, and (c) charged, (d) neutral species and electronic temperature with $t_s = 0.05$ s for p = 1.33 Pa, P_{RF} = 800 W, Q = 60 sccm constant, T_w=300 K Equivalent steady-state are reported as dots, while densities in dynamic mode as solid lines.

It is possible to timing out the feed gas composition and extract densities in order to compare with the steady-states. This allow us to discuss the lower limit of the divergence observed compared with Fig. 2, for a short feed gas switch duration t_s=0.05s.

In Fig. 8, for $t_s > 0.25$s, the densities calculated in dynamic mode are very close to those obtained in the steady-state. However, for shorter feed gas switch durations, significant divergences arise. The residual chlorine amount increases as the feed gas switch duration decreases, leading to an almost constant Cl density for the shortest feed gas

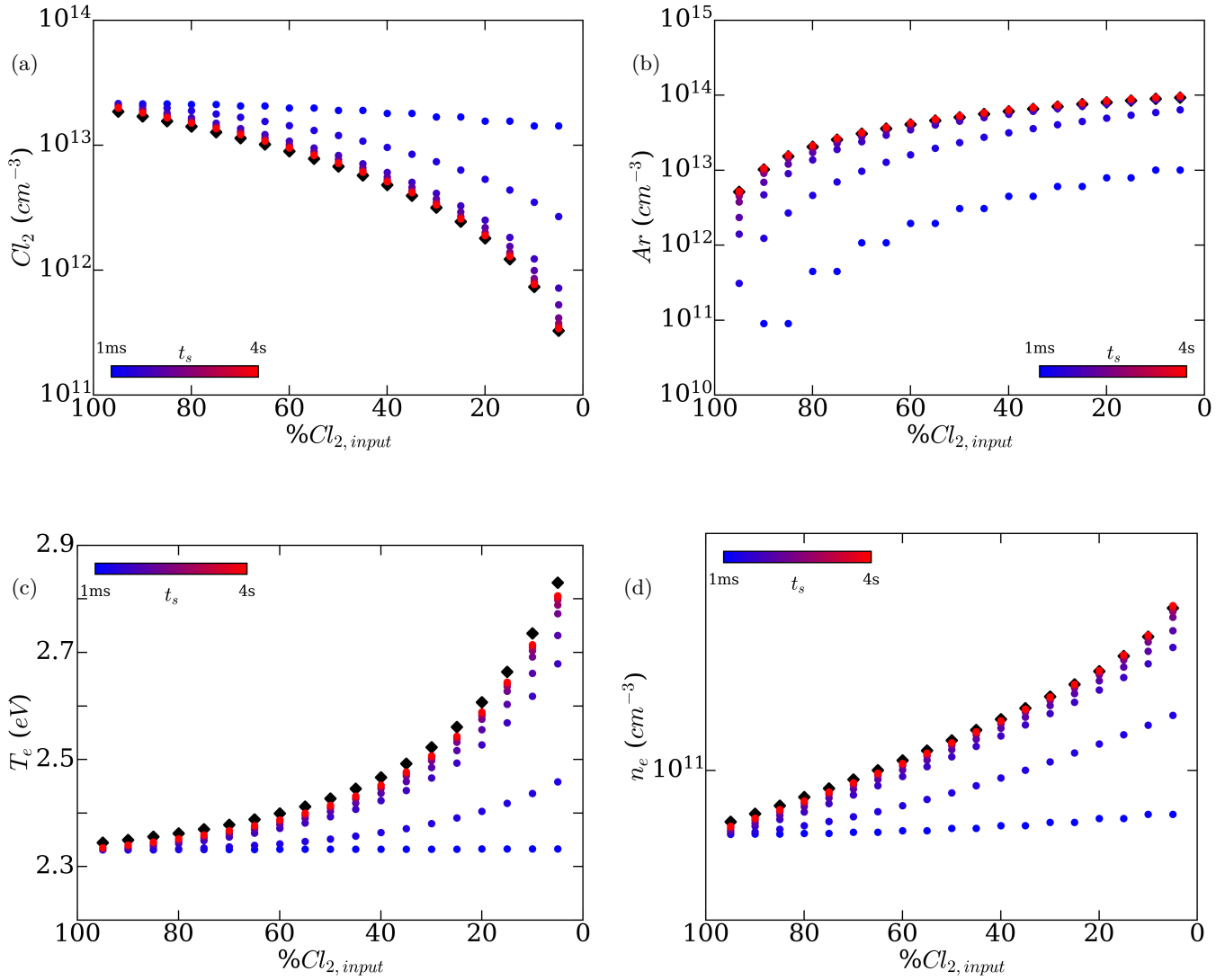

FIG. 8: Equivalent densities of (a) Cl_2, (b) Ar and (c) electron density and (d) electron temperature in dynamic mode versus $\%Cl_2$, compared with those in steady-state as black diamond markers at p = 1.33 Pa, P_{RF} = 800 W, Q = 60 sccm constant, T_w = 300 K.

switch duration of t_s = 0.001s.

Additionally, neutral argon, reported in Fig. 8-b, hardly increases at short feed gas switch durations. For the shortest feed gas switch duration, t_s= 0.001s, the neutral argon density is two orders of magnitude lower than the stationary states. Even if the input in the model imposed a density of the argon in source, the model for these fast composition transition, seems not to be able to properly substitute the chlorine densities. The origin of these observations will be discussed below.

Similarly, T_e and n_e both remain lower than their respective steady-states reported, in Fig. 8-c and -d, which

originate from the high residual chlorine in the plasma. As the plasma kinetic in our model is primarily governed by effective electron collisions, it is valuable to quantify these collisions during the feed gas switch from Cl to Ar for different durations.

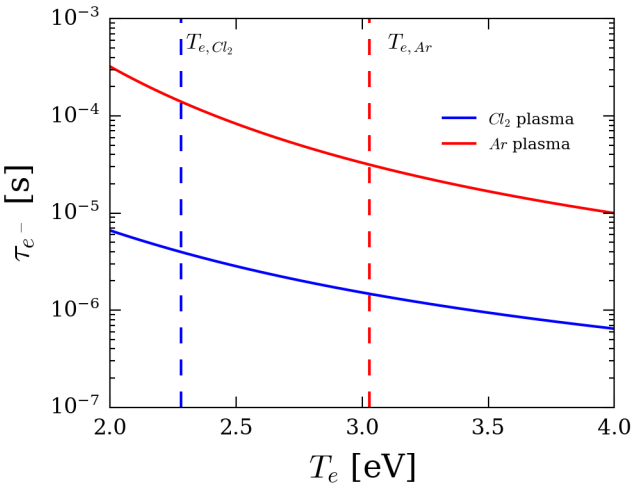

FIG. 9: Characteristic time of electronic collision in Cl_2 plasma and Ar plasma (blue and red lines respectively) as a function of the electron temperature for a plasma total density computed at p = 1.33 Pa, P_{RF} = 800 W, Q = 60 sccm constant and T_w = 300 K. We extrapolate the characteristic time of electronic collision as a function of T_e, with n=n_{tot} (in Cl_2 or Ar) constant with T_e. Vertical dashed lines represent the electronic temperature T_e in pure Cl_2 plasma and Ar plasma, in blue and red respectively computed at the same plasma parameters.

To quantify effective electronic collisions, we first calculate the global characteristic time of electronic collisions between an electron and any species present in a pure Cl_2 or a pure Ar plasma: atom, molecule, or ion. We defined the overall characteristic time of effective electronic collision reactions in the Cl_2 and Ar plasmas as :

$$\tau_{e/i} = \frac{1}{\sum k_i(T_e) \times n_{tot,i}} \tag{10}$$

where $\sum k_i(T_e)$ is the sum of kinetic coefficients of reactions by electronic collisions in i plasmas for i=Cl_2 or Ar. $n_{tot,i}$ is the total densities in the pure i plasma, in the steady-state mode.

The considered characteristic times of effective electronic collisions represent the average time between two collisions involving an electron and any gas species in the plasma, taking into account the reaction scheme of our model. The number of electrons involved in these collisions is weighted by the kinetic coefficients described in section 2.

In a pure Cl_2 plasma at p = 1.33 Pa, P_{RF} = 800 W, Q = 60 sccm and T_w = 300 K, the electronic temperature is T_{e,Cl_2} = 2.28 eV while in Ar plasma, T_{e,Cl_2} = 3.04 eV, reported as vertical dashed lines in blue and red, respectively

	Short t_s	Long t_s
$\mathbf{t_s}$ [s]	10^{-3}	1.0
$\mathbf{N_c}$	10^2	10^5
$\mathbf{n_{coll}}$ [cm^{-3}]	10^{13}	10^{16}

TABLE I: Compararison of electron collisions during short and long t_s. N^c is the number of collisions per electron during t_s and n^{coll} is the electron collision density during t_s

in Fig. 9. Proper total densities in Cl_2 and Ar plasmas are $n_{tot,Cl_2} = 1.31 \times 10^{14}$ cm^{-3} and $n_{tot,Ar} = 1.03 \times 10^{14}$ cm^{-3}. The higher total density for pure Cl2 plasma originates from dissociative processes in Cl2 plasmas.The dissociation of Cl_2 into Cl induces an increase of total pressure and total density in our model (one Cl_2 particle creates two distinct Cl particle). Consequently, the pressure in chlorine plasmas is greater than pure argon plasma. In transient plasma form Cl_2 to Ar, the change of total densities and pressure is the main reason for the implementation of a self-consistent description of the pressure in the model, described in Eq. 9.

In Fig. 9, we extrapolate the characteristic time of effective electronic collision as a function of T_e, with a constant total density (in Cl_2 or Ar) established under our calculation conditions. Thus, this value is valid only for the T_e used to calculate the total density, as the densities depend on T_e. The characteristic time of effective electronic collisions of Cl_2, from $\tau_{e/Cl_2} = 6.5 \times 10^{-6}$ s to 6.5×10^{-7} s, and Ar, from $\tau_{e/Ar} = 3.2 \times 10^{-4}$ s to 9.9×10^{-6} s, are both decreasing with T_e, from 2 eV to 4 eV, in Fig. 9. Higher kinetic energy leads to more effective collisions and therefore faster interactions. In addition, the characteristic time of Ar plasma is higher than that of Cl_2 because Ar plasma is less dense, leading to fewer electron-gas collisions.

These calculations lead to a characteristic time of effective electronic collision $\tau_{e/Cl_2} = 4 \times 10^{-6}$ s, in Cl_2 plasma and $\tau_{e/Ar} = 6 \times 10^{-5}$ s, in Ar plasma, for electron temperatures of 2.28 eV and 3.03 eV, respectively.

From these results, by approximating the characteristic time of electronic collisions for pure Ar and pure Cl_2 plasmas to $\tau_{e/tot} = 10^{-5}$ s, we can estimate, as shown in Table I, the number of effective electronic collisions during the feed gas switch from Cl_2 to Ar, for short and long durations: 0.001 s and 1 s, respectively.

Approximating the average characteristic time of effective electronic collisions at $\tau_{e/tot} = 10^{-5}$ s, we can determine the number of effective collisions per electron during the feed gas switch by dividing t_s by $\tau_{e/tot}$. We obtained a number of effective collisions per electron during the feed gas switch, $N_c = 10^2$ for $t_s = 0.001$ s and 10^5 for $t_s = 1.0$ s. By multiplying N_c by the averaged $n_e = 10^{11}$ cm^{-3}, we can deduce an electron collision density n_{coll}, occurring during the switch duration, $n_{coll} = 10^{13}$ cm^{-3} for $t_s = 0.001$ s and $n_{coll} = 10^{16}$ cm^{-3} for $t_s = 1$ s.

In comparison with the averaged plasma density, n_{tot} (10^{14} cm^{-3}) > n_{coll} (10^{13} cm^{-3}) when $t_s = 0.001$ s, the

calculated n_{coll} does not allow each gas particle to interact with an electron. This insufficiency may explain the discrepancies in the densities n_i and T_e obtained between dynamic mode results and steady-states conditions observed in Fig. 8 for $t_s < 0.25$ s.

Conversely, for a long feed gas switch duration ($t_s = 1$ s in Table I), we obtain n_{coll} (10^{16} cm^{-3}) > n_{tot} (10^{14} cm^{-3}). This two-order-of-magnitude difference allows each particle in the plasma to interact with an electron at least once, enabling the plasma to follow the gas change instructions.

This analysis implies the existence for our model of a cutoff time for t_s that allows the plasma to respond to the feed gas switch, explaining less differences between steady-state and dynamic results for $t_s > 0.25$ s in Fig. 8.

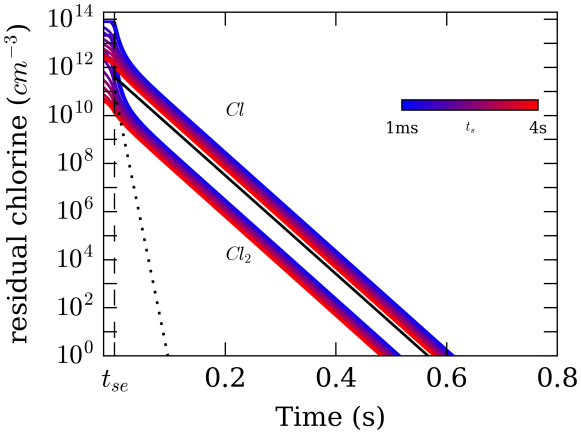

FIG. 10: Effect of t_s on Cl and Cl_2 densities at the end of the feed gas switch for t_s=[0.001,0.01,0.05,0.1,0.25,0.5,1,2,3,4] s at p = 1.33 Pa, P_{RF} = 800 W, Q = 60 sccm constant and T_w = 300K. t_{se} corresponds to the feed gas switch end, afterward, the feed gas is 100% Ar. Cl at the top and Cl_2 at the bottom. Solid black line corresponds to fitted function to obtain the characteristic time of the trends. Dotted line corresponds to residual chlorine density decay considering only the pumping term with the corresponding residence time τ_P.

In Fig. 10, we investigate the behaviors of Cl and Cl_2 densities at the end of the feed gas switch t_{se}, when the feed gas input is pure Ar. For each t_s simulation, the theoretical pure argon feed gas respective times, starting at t_{se}, have been shifted to 0s to allow a simultaneous comparison of Cl and Cl_2 behaviors. At each feed gas switch from Cl_2 to Ar, significant residual chlorine densities are observed in the argon plasma, as initially reported in Fig. 8.

Residual Cl and Cl_2 are important, even for the longest feed gas switch duration, from 1×10^{14} cm_3 to 4×10^{12} cm_3, for $t_s = 0.001$ s and $t_s = 4$ s respectively while Cl_2 goes from 8×10^{12} cm_3 to 5×10^{10} cm_3 , for $t_s = 0.001$ s and $t_s = 4$ s respectively. The amount of residual chlorine, Cl and Cl_2, decreases when increasing the feed gas switch duration. The longer the feed gas switch duration is, the better chlorine densities can accommodate to the extinction of the Cl_2 feed gas.

Chlorine densities show identical decreasing trends. The decreasing trends observed in Fig. 10 can be represented by an exponential decrease under the form of $exp(\frac{-t}{\tau_x})$, where τ_x is a characteristic time. We fitted the trends to extract the characteristic time of each species reported as the dotted lines in Fig. 10, with $\tau = 2.0\times\ 10^{-3}$ s.

For comparison, we reported on Fig. 10, as dotted lines, a decreasing exponential with a characteristic time equals to the pumping residence time calculated above τ_P. This one is factoring the reactor geometry, the flow rate and the pressure as described in Eq. 1. In our considered plasma conditions, the pumping residence time is $\tau_P = 3.8 \times 10^{-3}$s.

In order to evaluate the chlorine residual densities trends, from Eq. 1, we can approximate the mass balance equation by introducing the chemical characteristic time, by:

$$\frac{\partial n_i}{\partial t} \approx \pm\frac{n_i}{\tau_{C,i}} - \frac{n_i}{\tau_P} = -n_1\left(\pm\frac{1}{\tau_{C,i}} + \frac{1}{\tau_P}\right) \tag{11}$$

By solving the Eq. 11, we obtain:

$$n_i(t) = n_{i,0}\exp\left(-\frac{t}{\tau}\right) \tag{12}$$

where $\frac{1}{\tau} = \frac{1}{\tau_C} + \frac{1}{\tau_P}$ and $n_{i,0}$ is the n_i density at $t = t_{se} = 0$ s in this work, considering the variable change of t.

In this specific case, i represents Cl or Cl_2, $\tau_{C,i}$ corresponds to the chemical characteristic time which approximates the contribution of the plasma kinetic associated to electronic, inter-species and wall collisions. Noting that after t_{se}, the source term of Cl_2 feed gas is null.

From Fig. 10, we obtained a characteristic time for chlorine species decrease of $\tau = 2.0 \times 10^{-3}$ s. From Eq 11, we can deduce that $\tau_C = 4.64 \times 10^{-3}$ s, considering the pumping residence time $\tau_P = 3.8 \times 10^{-3}$ s. Both Cl and Cl_2 decays are slower than the pumping residence time indicating that these two species are still involve in chemical reactions in the pure Ar plasma and that the characteristic times of these reactions are longer than τ_P. Long lifetime of residuals species has been presumed to originate from surface recombination and reactions in the plasma volume[9]. The main reactions available for Cl_2 and Cl decays are chlorine dissociation (R0 : Cl_2 + e $\rightarrow$ 2Cl + e) and wall recombination (R230 : Cl + wall $\rightarrow \frac{1}{2}$ Cl_2). The slopes of Cl_2 and Cl densities are identical, suggesting that an equilibrium is established between these two reactions. They are highly sensitive to the pressure and the nature of plasma reactor walls.

As mentioned above, in order to be near the ALE conditions, we use the gas flow rate variations from Cl_2 to Ar represented in Fig. 1. Figure 11 presents the evolution of the electron temperature T_e during the feed gas switch

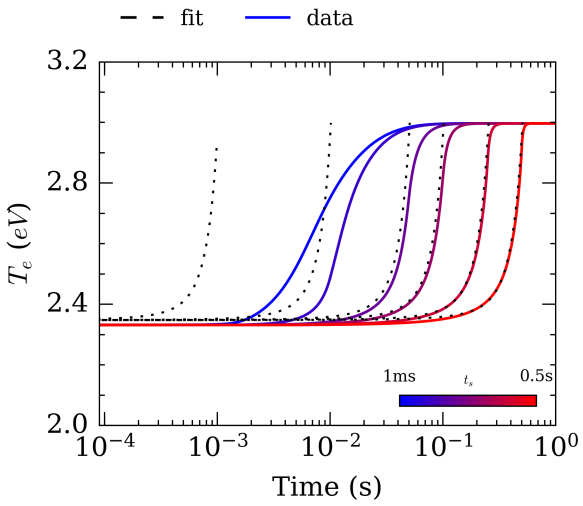

FIG. 11: Electron temperature during a gas source switch for different values of t_s=[0.001,0.01,0.05,0.1,0.25,0.5] s at p = 1.33 Pa, P_{RF} = 800 W, Q = 60 sccm constant and T_w=300 K

from Cl_2 to Ar for different switch duration t_s. As shown in the steady-state condition results, the transition from pure Cl_2 to pure Ar leads to an increase of T_e from a minimum value of 2.3 eV to a maximum 3.0 eV, corresponding to the T_e of pure Cl_2 and pure Ar, respectively. It should be noted that the minimum and the maximum values of T_e are independent of the transition duration and corresponds to the values obtained from the steady-state conditions. Almost exponential variation of T_e during the transitions are observed illustrating the nonlinear kinetic phenomena of the plasma discharge. The temporal variation of T_e in our transition duration range (Fig. 11) can be approximated by exponential function :

$$\begin{aligned} T_e(t) &= T_{e,min} + 0.0079 \times \exp\left(\frac{t - t_{sb}}{0.23 t_s}\right) \text{ for } t \leq t_{se} \\ T_e(t) &= T_{e,max} \text{ for } t \geq t_{se} \end{aligned} \tag{13}$$

where t_s is the transition duration and $t_{sb} = 0.5$ s is the start of the switch time. The switch from a Cl_2 plasma to Ar plasma is accompanied by an increase of T_e. At the switch beginning, T_e increases slowly, then a fast increase is observed, clearly, illustrating the exponential variation of T_e (see Eq. 13). This semi-empirical expression fits well the temporal evolution of T_e determined from the global kinetic model for $t_s > 0.1$ s, in agreement with aforementioned observations about discrepancies at very short t_s.

C. One ALE cycle

To be near the experimental conditions of ALE, we perform simulations in the same experimental conditions from a plasma ALE recipe by Mannequin et al.[33] trying to reproduce the plasma behavior. Highly chlorinated plasma is used for the modification step (40 sccm of Cl_2 and 10 sccm of Ar). Constant 10 sccm of argon plasma is applied during the entire cycle. In parallel, a constant RF source power is applied (50 W) for the purge and the modification steps while during the activation step, 120 W of RF power is applied to increase ion density (Fig. 12).

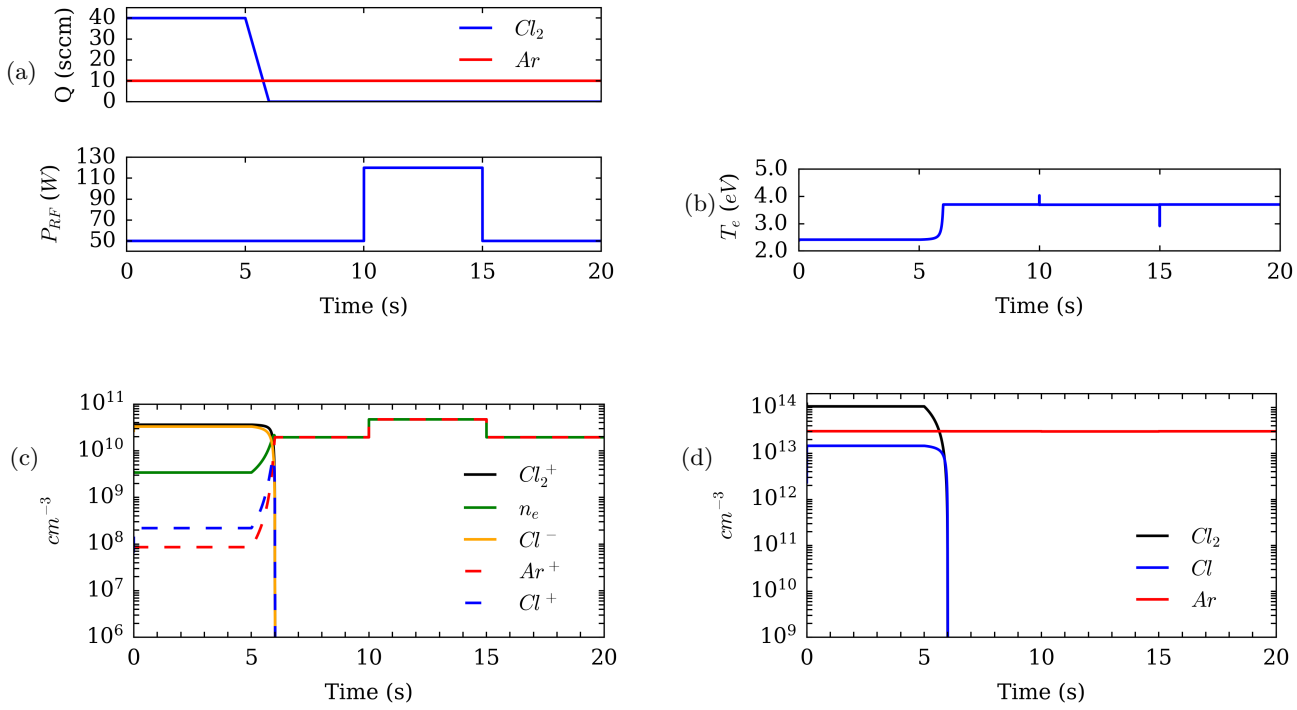

FIG. 12: Simulation of the Cl_2/Ar plasma in ALE conditions at p = 0.66 Pa, P_{RF} = 50 W and 120 W, T_w = 300 K and t_s = 1 s. (a) Flow rate and RF power parameters, (b) T_e, (c) charged species and (d) neutral species.

Simulation was carried out for a duration of 20 s corresponding to one cycle. Firstly, we considered an instantaneous switch from the Cl_2 gas source to Ar. In this case, a simulation discrepancy is observed which is characterized by the lack of evacuation of the chlorinated species during the purging steps in pure argon plasma. This can be justified by highly stiff numerical system of our global model.This abrupt switching from Cl_2 gas source to Ar induces a numerical instability leading to the wrong results. A feed gas switch duration t_s = 1 s prevent the divergence. Applying this feed gas switch duration in our model is not far from experimental conditions in the context of gas switch in a reactor that is not equipped with a pulsed gas injector.

During the first purge (5 to 10 s), the electron temperature increased from a higly chlorinated plasma to a pure Ar

plasma. T_e increases when Cl_2 switch from 100% to 0%. In addition, short bursts for T_e are observed at the beginning and the end of the added P_{RF} pulse during the activation step of the cycle. However, except during switching times, T_e does not undergo any variations, and it remains constant. This is consistent with the low sensitivity of T_e to P_{RF} variations reported in steady state.

Figure 12-c shows the charged species time evolution. n_e increases when moving from a highly chlorinated plasma to a pure argon plasma. This is in agreement with our previous results about plasma kinetics as a function of the feed gas composition in steady-state. However, there was a slight delay due to the presence of residual chlorine species.

In addition, we noted an instantaneous variation in n_e during the transition from the purge step to the activation step. As seen above, the ionization processes are more effective in the presence of Ar than of Cl_2. Furthermore, n_e increases during the transition from purge step to the activation step because of the increase of the RF power. On the other hand, Cl_2^+ and Cl^- are still the dominant ions during the modification step while the Cl^+ and Ar^+ densities are relatively weaker and almost equal. During the transition from the modification step to the purge step, a fast increase of Cl^+ and Ar^+ densities is observed because of the fast increase of the dissociative ionization rate of Cl_2 and the ionization of Cl and Ar due to the increase of n_e and T_e. In this transition phase, even if the neutral chloride population Cl_2 and Cl decreases, the fast increase of n_e and T_e leads to the fast increase of the ionization rate of Cl_2 and Cl to product Cl^+. At the end of the transition regime, Cl^+ density collapses while the Ar^+ continues to increase until reaching a constant value corresponding to the steady-state In Figure 12-d, we report the neutral species densities Cl_2,Cl and Ar species in the plasma during the ALE cycle. In these conditions Cl_2 density is above Cl density for the entire modification step, in opposition to our reported steady-state in Fig. 2 for p = 1.33 Pa and P_{RF} = 800 W. The low pressure of p = 0.66 Pa and P_{RF} = 50 W during the modification step, induce a lower chlorine dissociation.

D. ALE multicycle

Experimental ALE cycles are numerous, even hundreds during an etching process. To ensure the reproductibility of our results over several ALE cycles, we consider 10 successive ALE cycles by applying a linear switchover from Ar to Cl_2 gas flow over a period of 1s at the end of each ALE cycle.

Figure 13 reveals the excellent reproducibility of our model over a sequence of 10 ALE cycles. The amplitudes and trends in the evolution of species densities are exactly the same from one cycle to the next, and cycles can almost be

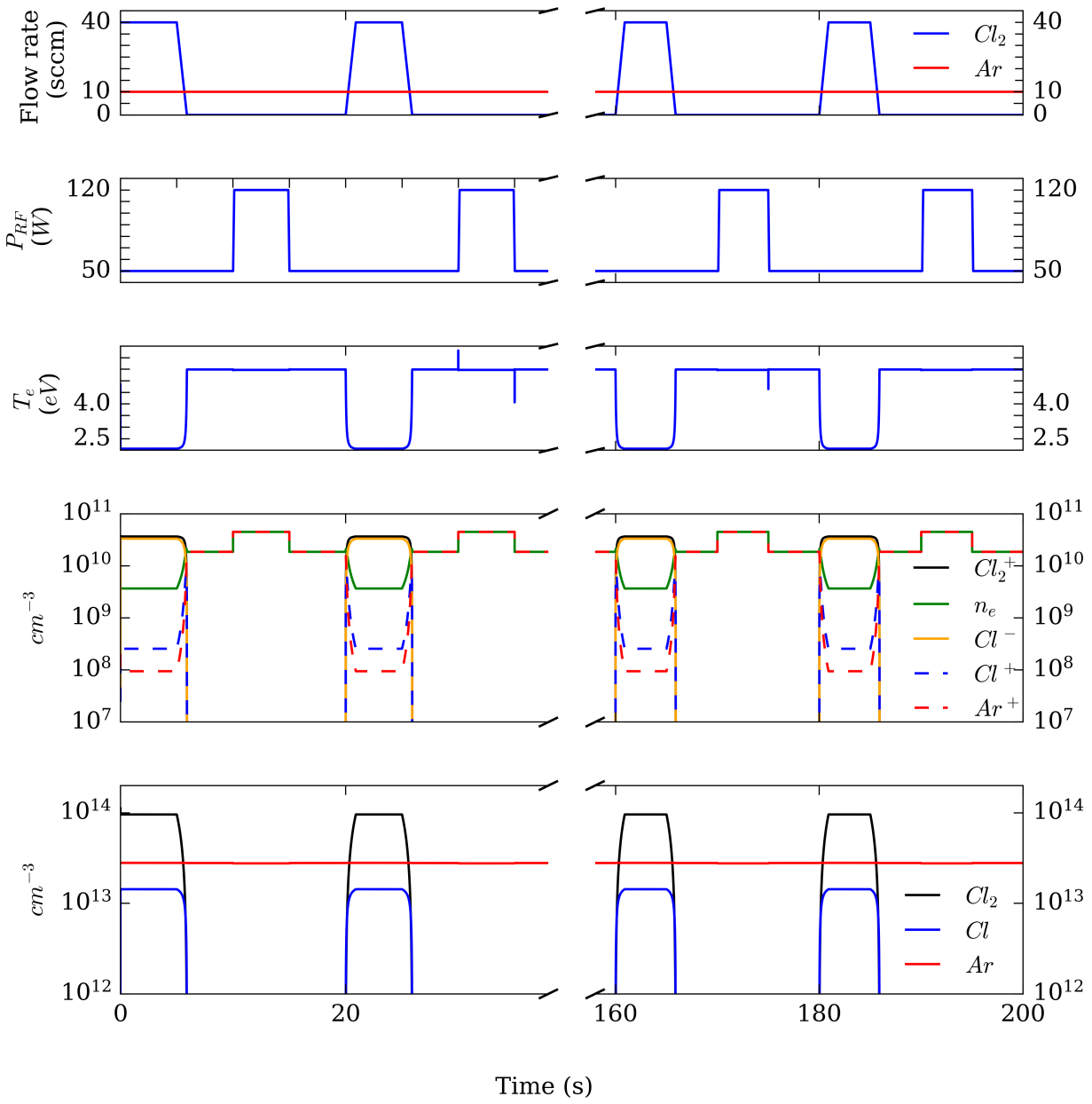

FIG. 13: Modelling of the Cl_2/Ar plasma for 10 successive ALE of GaN in chlorinated plasma for P_{RF} = [50 W,120 W], p = 0.66 Pa, T_w = 300 K, t_s = 1 s.

considered independent. Each cycle has the same input machine parameters illustrating the ALE process. However, we aimed to quantify the impact of preceding cycles on subsequent ones. In our study, ALE steps last for 5 seconds, the plasma kinetics could be delayed if $t_s < 0.5$ s. This allows the good system response to the perturbations induced by the feed gas and source power switches. Consequently, the accumulation of errors induced by previous steps can be neglected, and each simulated cycle appears to be independent. Concerning the densities of species present in the reactor, their variations are symmetricals between the $Cl_2 \rightarrow$ Ar and Ar $\rightarrow Cl_2$ plasma source switches. Cl^+ maxima

can be observed in weakly chlorinated plasmas either during $Cl_2 \rightarrow Ar$ or $Ar \rightarrow Cl_2$ transitions, observed initially in the stationary states and then during a change of plasma source in the previous sections.

IV. CONCLUSION

A Cl_2/Ar plasma dynamic global model is developed and applied to provide insights on plasma kinetics during pulsed processes, such as Atomic Layer Etching (ALE) conditions. The advantage of our model lies in its ability to track the time evolution of neutral and ion species densities, considering alternating feed gases. We first compared our results with the literature to validate the reaction scheme and the kinetics in steady-state, showing satisfactory agreements. Our initial results of the temporal ramp of composition change in the Cl_2/Ar feed gas align well with the steady-state ones, provided the feed gas switch duration ts is sufficiently long. In plasmas primarily driven by electron interactions, the feed gas switch duration must exceed a minimum limit ($t_s > 0.1$ s) to ensure adequate effective electron collisions for responsiveness to input parameters. Significant residual chlorine densities are observed after switching from Cl_2 plasma to Ar plasma, independent of the feed gas switch duration, lasting several hundred milliseconds, highlighting the existence of a chemical characteristic time presumed to be maintained by a balancing between reactions at the plasma volume and wall recombination. During the ALE cycle, Cl^+ reaches its maximum around 15% Cl_2, indicating a critical result regarding the need for chlorine adsorption during the modification step rather than the purge. Finally, we modeled a chain of ALE cycles. The presence of purge steps between modification and activation prevents residual chlorine during the activation step. Setting each step to 5 seconds ensures the stability of plasma kinetics and no diffusion discrepancies.

ACKNOWLEDGMENTS

This study is financially supported by STMicroelectronics Tours, France.

Appendix A: Appendixes

Data availlability

The data that support the findings of this study are available within the article. Supplementary informations are available (reaction scheme, complete results of calculations)

Conflict of interest

The authors have no conflicts to disclose.

REFERENCES

[1]V. M. Donnelly and A. Kornblit, "Plasma etching: Yesterday, today, and tomorrow," Journal of Vacuum Science & Technology A **31**, 050825 (2013).

[2]W. Saito, M. Kuraguchi, Y. Takada, K. Tsuda, I. Omura, and T. Ogura, "Influence of surface defect charge at AlGaN-GaN-HEMT upon Schottky gate leakage current and breakdown voltage," IEEE Transactions on Electron Devices **52**, 159–164 (2005).

[3]K. J. Kanarik, T. Lill, E. A. Hudson, S. Sriraman, S. Tan, J. Marks, V. Vahedi, and R. A. Gottscho, "Overview of atomic layer etching in the semiconductor industry," Journal of Vacuum Science & Technology A: Vacuum, Surfaces, and Films **33**, 020802 (2015).

[4]T. Matsuura, J. Murota, Y. Sawada, and T. Ohmi, "Self-limited layer-by-layer etching of Si by alternated chlorine adsorption and Ar+ ion irradiation," Applied Physics Letters **63**, 2803–2805 (1993).

[5]S. D. Athavale and D. J. Economou, "Realization of atomic layer etching of silicon," Journal of Vacuum Science & Technology B: Microelectronics and Nanometer Structures Processing, Measurement, and Phenomena **14**, 3702–3705 (1996).

[6]S. Tan, W. Yang, K. J. Kanarik, T. Lill, V. Vahedi, J. Marks, and R. A. Gottscho, "Highly Selective Directional Atomic Layer Etching of Silicon," ECS Journal of Solid State Science and Technology **4**, N5010–N5012 (2015).

[7]A. Goodyear and M. Cooke, "Atomic layer etching in close-to-conventional plasma etch tools," Journal of Vacuum Science & Technology A: Vacuum, Surfaces, and Films **35**, 01A105 (2017).

[8]Q. Hao, P. Kim, S. K. Nam, S.-Y. Kang, and V. M. Donnelly, "Real-time monitoring of atomic layer etching in Cl2/Ar pulsed gas, pulsed power plasmas by optical emission spectroscopy," Journal of Vacuum Science & Technology A **41**, 032605 (2023).

[9]A. Fathzadeh, P. Bezard, M. Darnon, I. Manders, T. Conard, I. Hoflijk, F. Lazzarino, and S. de Gendt, "Transient-assisted plasma etching (TAPE): Concept, mechanism, and prospects," Journal of Vacuum Science & Technology A **42**, 033006 (2024).

[10]T. Ohba, W. Yang, S. Tan, K. J. Kanarik, and K. Nojiri, "Atomic layer etching of GaN and AlGaN using directional plasma-enhanced approach," Japanese Journal of Applied Physics **56**, 06HB06 (2017).

[11]H. Fukumizu, M. Sekine, M. Hori, K. Kanomaru, and T. Kikuchi, "Atomic layer etching of AlGaN using Cl2 and Ar gas chemistry and UV damage evaluation," Journal of Vacuum Science & Technology A: Vacuum, Surfaces, and Films **37**, 021002 (2019).

[12]T. J. Sommerer and M. J. Kushner, "Monte Carlo-fluid model of chlorine atom production in Cl2, HCl, and CCl4 radio-frequency discharges for plasma etching," Journal of Vacuum Science & Technology B: Microelectronics and Nanometer Structures Processing, Measurement, and Phenomena **10**, 2179–2187 (1992).

[13]C.-C. Hsu, M. A. Nierode, J. W. Coburn, and D. B. Graves, "Comparison of model and experiment for Ar, Ar/O $_{222}$$ inductively coupled plasmas," Journal of Physics D: Applied Physics **39**, 3272–3284 (2006).

[14]B. Ramamurthi and D. J. Economou, "Two-dimensional pulsed-plasma simulation of a chlorine discharge," Journal of Vacuum Science & Technology A: Vacuum, Surfaces, and Films **20**, 467–478 (2002).

[15]C. S. Corr, E. Despiau-Pujo, P. Chabert, W. G. Graham, F. G. Marro, and D. B. Graves, "Comparison between fluid simulations and experiments in inductively coupled argon/chlorine plasmas," Journal of Physics D: Applied Physics **41**, 185202 (2008).

[16]S. Ashida, C. Lee, and M. A. Lieberman, "Spatially averaged (global) model of time modulated high density argon plasmas," Journal of Vacuum Science & Technology A: Vacuum, Surfaces, and Films **13**, 2498–2507 (1995).

[17]R. Chanson, A. Rhallabi, M. C. Fernandez, C. Cardinaud, and J. P. Landesman, "Modeling of inductively coupled plasma Ar/Cl2/N2 plasma discharge: Effect of N2 on the plasma properties," Journal of Vacuum Science & Technology A: Vacuum, Surfaces, and Films **31**, 011301 (2013).

[18]R. Chanson, A. Rhallabi, M. C. Fernandez, and C. Cardinaud, "Modeling of InP Etching Under ICP Cl $_{222}$ on the Etch Anisotropy Evolution," Plasma Processes and Polymers **10**, 213–224 (2013).

[19]A. Rhallabi, R. Chanson, J.-P. Landesman, C. Cardinaud, and M.-C. Fernandez, "Atomic scale study of InP etching by Cl $_2$ -Ar ICP plasma discharge," The European Physical Journal Applied Physics **53**, 33606 (2011).

[20]S. C. McNevin, "Radio frequency plasma etching of Si/SiO2 by Cl2/O2 : Improvements resulting from the time modulation of the processing gases," Journal of Vacuum Science & Technology B: Microelectronics Processing and Phenomena **8**, 1185–1191 (1990).

[21]E. Despiau-Pujo, M. Brihoum, P. Bodart, M. Darnon, and G. Cunge, "Pulsed Cl $_2$ /Ar inductively coupled plasma processing: 0d model versus experiments," Journal of Physics D: Applied Physics **47**, 455201 (2014).

[22]G.-H. Kim, A. Efremov, D.-P. Kim, and C.-I. Kim, "Inductively coupled Cl2/N2 plasma: Experimental investigation and modeling," Microelectronic Engineering **81**, 96–105 (2005).

[23]A. Efremov, G.-H. Kim, J.-G. Kim, A. Bogomolov, and C.-I. Kim, "Applicability of self-consistent global model for characterization of inductively coupled Cl2 plasma," Vacuum **81**, 669–675 (2007).

[24]S. Kawano, K. Nanbu, and J. Kageyama, "Systematic simulations of plasma structures in chlorine radio frequency discharges," Journal of Physics D: Applied Physics **33**, 2637–2646 (2000).

[25]S. Huang and J. T. Gudmundsson, "A particle-in-cell/Monte Carlo simulation of a capacitively coupled chlorine discharge," Plasma Sources Science and Technology **22**, 055020 (2013).

[26]S. Huang and J. T. Gudmundsson, "Ion Energy and Angular Distributions in a Dual-Frequency Capacitively Coupled Chlorine Discharge," IEEE Transactions on Plasma Science **42**, 2854–2855 (2014).

[27]G. Le Dain, F. Laourine, S. Guilet, T. Czerwiec, G. Marcos, C. Noel, G. Henrion, C. Cardinaud, A. Girard, and A. Rhallabi, "Etching of iron and iron–chromium alloys using ICP-RIE chlorine plasma," Plasma Sources Science and Technology **30**, 095022 (2021).

[28]P. J. Chantry, "A simple formula for diffusion calculations involving wall reflection and low density," Journal of Applied Physics **62**, 1141–1148 (1987).

[29]E. G. Thorsteinsson and J. T. Gudmundsson, "A global (volume averaged) model of a chlorine discharge," Plasma Sources Science and Technology **19**, 015001 (2010).

[30]K. R. Alan C. Hindmarsh, "Description and Use of LSODE, the Livermore Solver for Ordinary Differential Equations," **LLNL report UCRL-ID-113855** (1993).

[31]G. Franz, "Comprehensive analysis of chlorine-containing capacitively coupled plasmas," Journal of Vacuum Science & Technology A **23**, 369–387 (2005).

[32]N. C. M. Fuller, I. P. Herman, and V. M. Donnelly, "Optical actinometry of Cl2, Cl, Cl+, and Ar+ densities in inductively coupled Cl2–Ar plasmas," Journal of Applied Physics **90**, 3182–3191 (2001).

[33]C. Mannequin, C. Vallée, K. Akimoto, T. Chevolleau, C. Durand, C. Dussarrat, T. Teramoto, E. Gheeraert, and H. Mariette, "Comparative study of two atomic layer etching processes for GaN," Journal of Vacuum Science & Technology A **38**, 032602 (2020).

[34]S. Tinck, W. Boullart, and A. Bogaerts, "Modeling Cl $_22$ /Ar inductively coupled plasmas used for silicon etching: effects of SiO $_2$ chamber wall coating," Plasma Sources Science and Technology **20**, 045012 (2011).

[35]T. J. Flack, B. N. Pushpakaran, and S. B. Bayne, "GaN Technology for Power Electronic Applications: A Review," Journal of Electronic Materials **45**, 2673–2682 (2016).

[36]J. Ladroue, A. Meritan, M. Boufnichel, P. Lefaucheux, P. Ranson, and R. Dussart, "Deep GaN etching by inductively coupled plasma and induced surface defects," Journal of Vacuum Science & Technology A **28**, 1226–1233 (2010).

[37]T. List, T. Ma, P. Arora, V. M. Donnelly, and S. Shannon, "Complex transients in power modulated inductively-coupled chlorine plasmas," Plasma Sources Science and Technology **28**, 025005 (2019).

[38]H. H. Cosby P C, "DISSOCIATION RATES OF DIATOMIC MOLECULES," US Air Force Material Command, Wright Patterson AFB (1992).